4 Results and Discussions

4.1 General Consideration

In this chapter, results will be presented and discussed. Further, if possible, they will be compared with mean-field results. As mentioned in previous chapters, the interest is especially in the interfacial properties of asymmetric polymer blends and their phase behavior.

The interfacial properties of polymers with various degrees of flexibilities are discussed in section 4.2. The systems consist of flexible and semiflexible polymers whose flexibility varies fom flexible polymers to stiff rod. Various quantities which characterize the polymer-polymer interface have been studied. The interfacial tension as a function of statistical segment length of semiflexible component has been calculated using virial theorem and capillary wave spectrum method. Simulation results are compared with the mean field results of Helfand and Sapse [20], and Liu and Fredrickson [67]. Similarly, the interfacial width as a function of stiffness of semiflexible chains is studied by simulation and they are compared with the mean field results of Helfand-Sapse and Liu-Fredrickson. The monomer density profiles are also obtained as a function of chain stiffness of semiflexible components. Further, we study the orientaions of chains and bonds. The other interfacial properties which characterize the interface are distribution of chain ends and center of mass of polymer chains. All of these quantities are studied as a function of chain stiffness of semiflexible component.

In section 4.3, the interface properties of polymers with different monomer sizes will be presented. We study and compare our results for interfacial properties of two different types of systems; (1) a system having two different types (say type A and type B) of polymer chains such that the diameter of a type B monomer is double than that of type A monomer but the number of monomers per chain for both types of polymers is equal i.e, "monomer size disparity with equal number of monomers per chain" , and (2) a system having two different types (say type A and type B) of polymer chains with almost equal radius of gyration, however, the diameter of type B monomers is double than that of type A monomers. The results of such asymmetric polymer-polymer interfaces are compared to the interfacial properties of symmetric system in which the size of monomers of both types of chains as well as number of monomers per chain are equal. The simulation results are compared with mean field results of Helfand and Sapse [20].

Other interfacial properties like density profile, chain orientation, distribution of chain ends near the interface and distribution of center of mass of polymer chains are also studied.

In section 4.4, we estimate the critical value of Flory-Huggins parameter as a function of degree of chain flexibility in a system of flexible-semiflexible polymers such that semiflexible chains are far from isotropc-nematic transition. In simulation, one can study phase diagram of polymer mixture by using semi-grandcanonical techniuqes in which types of chains are fluctuating but total number of particles remains constant. Because of high stiffness disparity for our systems of study such techniques will be inefficient for the present study. By calculating interfacial tension for weak segregation limit, we estimate the value of Flory-Huggins parameter χ at which the interfacial tension becomes zero, corresponding value of χ is critical value of χ at which two types of polymers get phase separated.

4.2 Interfaces of Flexible and Semiflexible Polymers

In this section we describe the results about the interface properties of flexible and semiflexible polymers at strong segregation limit. As mentioned before the present study covers the whole range of flexiblity of semiflexible polymers from flexible to stiff rods. We have studied interfacial tension, interfacial width, density profile, distribution of chain ends near the interface, distribution of center of mass of polymers near the interface, orientation of chains and bonds near the interface as a function of stiffness of the semiflexible chains. All these results will be presented and discussed in following subsections.

4.2.1 Interfacial Tension

Fig. 4.1 shows the obtained results for the interfacial tension of an interface between chains without additional bending restrictions and semiflexible chains described in previous chapter versus the statistical segment length of the stiffer chains estimated according to Eq. 3.4. The results obtained by the virial theorem and by the capillary wave method agree very well within the error bars estimated by the fluctuations of the single measurements (see above). The interfacial tension increases with increasing stiffness of the semiflexible component and levels of for values of stiffness beyond the semiflexible region $b \ll L$ which is visible also by the violation of the relationship $b = 2l_p - 1$ in Table 3.1. In Fig. 4.1 also simulation results obtained by Mueller and Werner [38] within the bond-fluctuation model for a rather limited range of stiffness disparity are displayed.

The interfacial tensions obtained by using virial theorem are higher than that by capillary wave spectrum method. This systematic difference can be attributed to the fact that virial theorem gives the difference of free energy per cross sectional area of the interface while capillary method is related to the interfacial area. Therefore, a little bit

higher interfacial tension obtained by virial theorem is not unexpected.

In the simulation results it can be seen that there is a very strong tendency towards saturation of interfacial tension with increasing statistical segment length of semiflexible components. Moreover, from these results it can be seen that there is no change in the saturation property of interfacial tension even though the statistical segment length of semiflexible component crosses the isotropic-nematic transition region and hence we are dealing with isotropic-nematic (flexible-stiff rod) interface instead of isotropic-isotropic interface, provided in the isotropic-nematic interface the polymers forming nematic phase are parallel to the interface plane (when one considers the isotropic-nematic interface the interfacial tension (in fact, interfacial properties) depend on the direction of orientation of polymers which form the nematic phase [75]. In the present work, only one case of the isotropic-nematic interface of flexible-stiff poylmers is considered in which the nematic director is parallel to the interface. The interfacial tension gets saturated before the stiffer chains form nematic phase and this trend of interfacial tension continues. The profile of interfacial tension against the statistical segment length of semiflexible component is very smooth after segment length in our model crosses the value 6.07.

These simulation results are compared with the mean-field results of Helfand and Sapse [20], and Liu and Fredrickson [67].

Helfand and Sapse [20] obtained for the interfacial tension, σ, of a planar interface between two phases of Gaussian chains with different statistical segment lengths interacting via a Flory-Huggins-type interaction

$$\frac{\sigma}{k_B T} = \frac{2}{3}\sqrt{\alpha}\left(\frac{(\beta_A^3 - \beta_B^3)}{(\beta_A^2 - \beta_B^2)}\right) \tag{4.1}$$

The β_i ($i = A, B$)

$$\beta_i = \sqrt{\frac{1}{6}\rho_{0i} b_i} \tag{4.2}$$

are the parameters which contain the chain statistics. The statical segment lengths b_i are defined in the same way as in Eq. 3.4 and the ρ_{0i} are the number densities of statistical segments in both bulk phases respectively. For comparison with simulation data we will use the mapping

$$\rho_{0i} = \frac{\rho_0}{C_{\infty i}} \tag{4.3}$$

which corresponds to the introduction of statistical segments by Eq. 3.4. ρ_0 is then the number density of beads which is the same for both chains. The interaction parameter α of the interaction between two statistical segments is then given by

$$\alpha = \rho_0 \chi \tag{4.4}$$

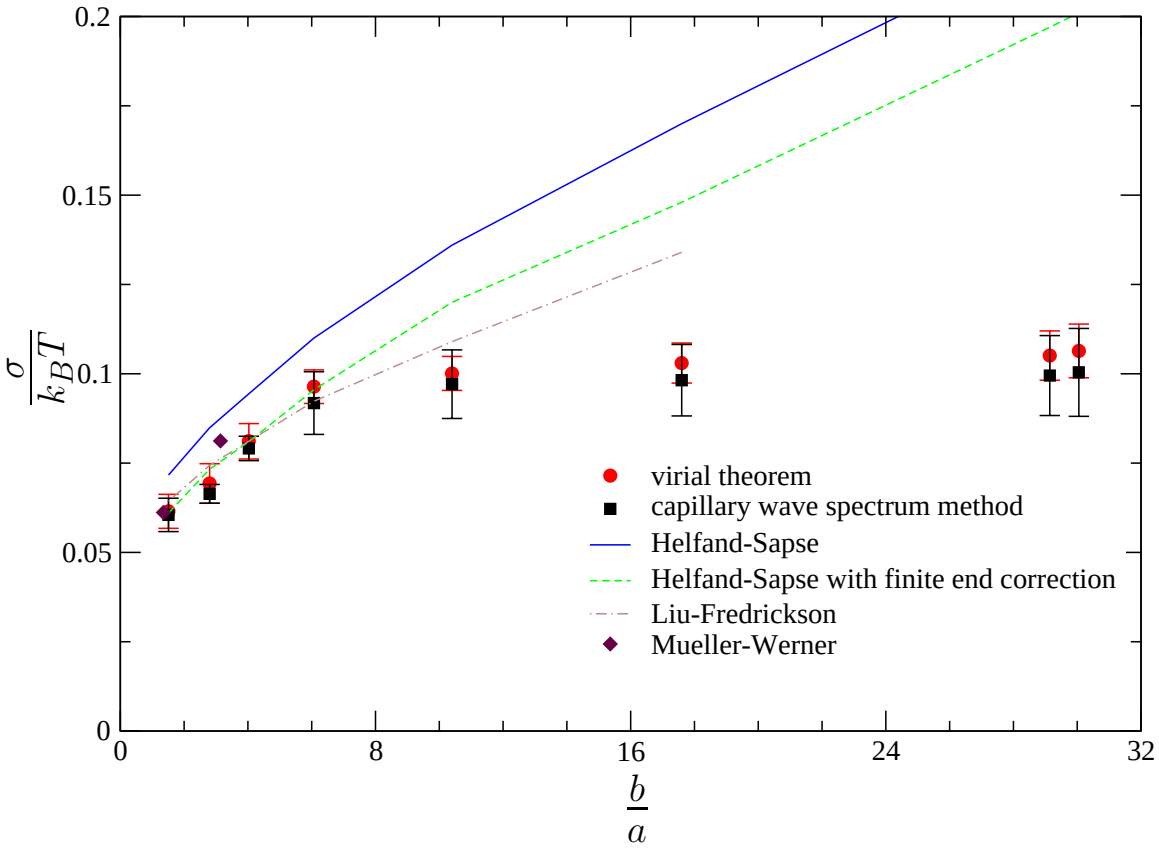

Figure 4.1: Interfacial tension as a function of statistical segment length of semiflexible polymers. The statistical segment lengths are in units of average bond length.

with the Flory-Huggins-parameter χ for the interaction of two beads of chains of different kind as defined by Eq. 3.3. For the interfacial tension of chains with the same segment length the Helfand Tagami result [65],

$$\frac{\sigma}{k_BT} = \rho_b b \sqrt{\frac{\chi_b}{6}} \tag{4.5}$$

is reproduced with now ρ_b and χ_b as the number density and interaction parameter of statistical segments. Fig. 4.1 shows clearly that the Helfand-Sapse results [20] agree well with the simulation data in the really semiflexible range of our system but differs increasingly with increasing stiffness. Expected reasons are as well effects of finite chain length as also the formation of local order with increasing stiffness. It will be discussed below.

Liu and Fredrickson [67] analyzed the interfacial tension of binary blends of polymers with different stiffness starting from a wormlike chain hamiltonian for both chains and with an interaction hamiltonian quadratic in both order parameters, concentration and orientation. Using a Landau-de Gennes expansion for the orientational part of the free

energy, fixing the value of the Maier-Saupe parameter and assuming weak orientation only, they obtained;

$$\frac{\sigma}{k_B T} = \frac{4}{9a_0^2}\sqrt{\chi}\frac{\kappa_A^{3/2} - \kappa_B^{3/2}}{\kappa_A - \kappa_B} \tag{4.6}$$

where a_0 is the monomer length and κ_i ($i = A, B$) is the dimensionless persistence length (in units of a_0) of the ith component of the polymer blend. Eq. 4.6 has the drawback showing not the expected dependence on monomer density as eg Eqs. 4.1 and 4.5 and also not agreeing with Eq. 4.5 in the limiting case $\kappa_A = \kappa_B = 1$.

Using the correction factor $\sqrt{\frac{3}{8}}$ proposed in [67], with the replacement $\kappa = \frac{C_{1N}+1}{2}$ and using our values for the average bond length as monomer length i.e., $a_0 \sim a \sim 2l_c$ for two flexible chains, we get almost complete numerical agreement with the results from Eq. 4.5. With this choice of parameters the interfacial tension according to Eq. 4.6 in Fig. 4.1 shows a less increase with increasing stiffness disparity as the Helfand-Sapse result [20] and seems to agree better with the simulation result for large stiffness. But the above discussed problems and the behavior at small stiffness disparities rules Eq. 4.6 out to be a suitable expression for describing the interfacial tension for unsymmetrical polymer blends.

Up to now, the simulation results for finite segment numbers are compared with mean-field results for long chains. In literature (see e.g. [87]) several corrections for finite segment numbers are discussed. Ermoshkin and Semenov [87] reconsidered the problem most recently and proposed corrections for interfaces between blends with different molecular weight and also for the case $\chi N \sim 1$. Using the correction $(1 - 4\frac{\ln 2}{\chi N})$ obtained in [87] to Eq. 4.1 the reduction is too large but we get an almost complete agreement for the region of small stiffness disparity using the correction factor $(1 - 2\frac{\ln 2}{\chi N})$ obtained in [88] as is visible from Fig. 4.1. A detailed discussion of possible physical reasons for this disagreement is beyond the scope of this work but it may be related to the problem already discussed by Binder [1] that a minimization of a free energy functional in square gradient approximation is not sufficient for the strong segregation case $\chi N > 1$.

As main reason for the differences between mean-field results and simulation at higher stiffness disparities the strong orientation of bonds and chains near the interface must be considered (see below). This is not taken into account in the approaches discussed above. Moreover, when the persistence length $(\frac{l_p}{a})$ of semiflexible chains is beyond ≈ 13.6 an isotropic-nematic transition will occur (see table 3.1). This strong increase in order in bulk is not accompanied by a visible change in the stiffness-dependence of the interfacial tension. This is an additional hint that the orientation near the interface is already large in the case of isotropic bulk phases and determines the stiffness dependence of interfacial tension. To derive the formula 4.6, Liu and Fredrickson assumed that the semiflexible polymers, in flexible-semiflexible polymer system, are far from nematic phase. By increasing the persistence length of semiflexible component, the system will be closer to isotropic-nematic transition. Therefore, the disagreement with their results

for the system with flexible and highly stiff polymer chains is not unexpected. Further in their study, they fix Maier-Saupe parameter. When we increase the stiffness parameter of semiflexible chains the Maier-Saupe parameter of semiflexible chains also increases. These could be the reasons why the difference between mean-field and simulation goes on increasing with the stiffness of semiflexible component.

4.2.2 Density Profile and Interfacial Width

The entanglements in the interfacial zone are of major importance for the mechanical properties of the blend. Therefore, the monomer density profiles of different components of the polymer blends are also important. Figure 4.2 presents the density profiles of the individual components as well as total monomer density profile as a function of the stiffness parameter of the semiflexible component. The density profiles for the different stiffness parameters are not much different until the persistence length ($\frac{l_p}{a}$) of semiflexible component is 13.6. The profiles become sharper in the semiflexible side as the stiffness increases. When the persistence length ($\frac{l_p}{a}$) of the semiflexible components is larger than 13.6, it forms a nematic phase and the density profiles also become quite different and molecularly sharp which clearly shows decrease in interfacial width significantly. We can describe these profiles also by the tangent hyperbolic function 3.28. For example, figure 4.2 shows the tangent hyperbolic function fitted for the system with flexible-semiflexible polymers in which semiflexible component has persitence length ($\frac{l_p}{a}$) =2.5. A reduction of the total monomer density is observed at the center of the interface and the effect increases with the increase in the stiffness of semiflexible component. When the persistence length ($\frac{l_p}{a}$) of the semiflexible component of polymers is more than 13.6 the reduction of the total monomer density at the interface is very high as shown in the figure 4.2. The minimum value of total monomer density is 0.95 in the case of persistence length ($\frac{l_p}{a}$) of semiflexible component 13.6 whereas it is about 0.85 and 0.63 for the systems with isotropic-nematic interfaces with persistence length ($\frac{l_p}{a}$) of semiflexible component 28.0 and 30.02 see figure 4.3. It should be noted that in the present work, the nematic director in isotropic-nematic interface is parallel to the interface plane. Thus it is observed that as the stiffnes of the semiflexible component increases the density profile becomes sharper in semiflexible side and the depth of dip in the total density at the interface goes on increasing.

These results qualitatively agree with the previous results of Schmid and Mueller [66] for symmetric polymer-polymer interface and results of Liu and Fredrickson [67]. However, Mueller and Werner [38] have reported that the reduction of the total monomer density at the center of the interface is almost independent of the stiffness of the semiflexible component and the density profiles for stiffness disparity are almost independent of stiffness of semiflexible component. The reason may be that they considered very small stiffness disparity ($C_{1N} = 3.13$ is highest characteristic ratio, estimated from their data), therefore, in their results the reduction of total monomer density at the center of the interface is almost independent of stiffness. In the present results also if we just

consider very small stiffness disparity as in their case (e.g. statistical segment length of semiflexible component = 1.51 and 2.8 only), we cannot see the small difference in the reduction of total monomer density at the center of the interface and density profiles are also almost independent of statistical segement length of semiflexible component which agrees very well with their results up to the stiffness disparity they studied. Comparing the flexible-flexible polymer interface with the interface of flexible polymers and semiflexible polymers with persistence length ($\frac{l_p}{a}$) 13.6, the amount of reduction of total monomer density at the interface is little different and the density profiles are also not much different.

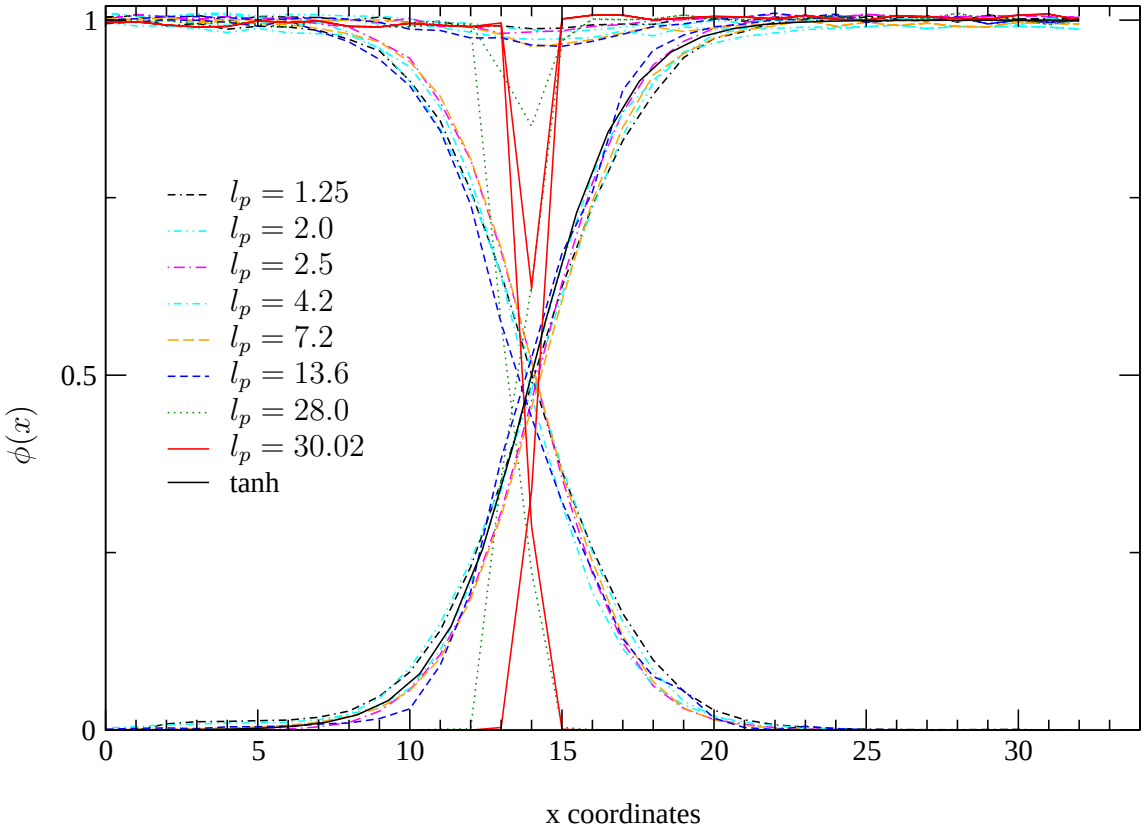

Figure 4.2: Normalized total monomer density and individual component density as a function of chain stiffness of the semiflexible polymers. Persistence lengths l_ps are in unit of average bond length. $\phi(x)$ is the normalized monomer density. Tangent hyperbolic function describing $\phi(x)$ of the system with $\frac{l_p}{a}$ = 2.5 is also shown.

The total interface width w (compare to Eq. 3.27) is determined as already explained

in 3.4 by fitting the density profile to the model function 3.28. The intrinsic width w_0 follows then analyzing Eq. 3.27. As already discussed above as lower cutoff length the minimum of persistence length l_p is used. We get a slight decrease of total interface width with increasing stiffness disparity within the range of an isotropic phase for the semiflexible chains but a sharp decrease down to a molecularly sharp interface as visible in Figure 4.2 for the interface between flexible chains and stiff chains in nematic state. Figugre 4.4 shows also the data for the intrinsic width (considering persistence length as the lower cut off length).

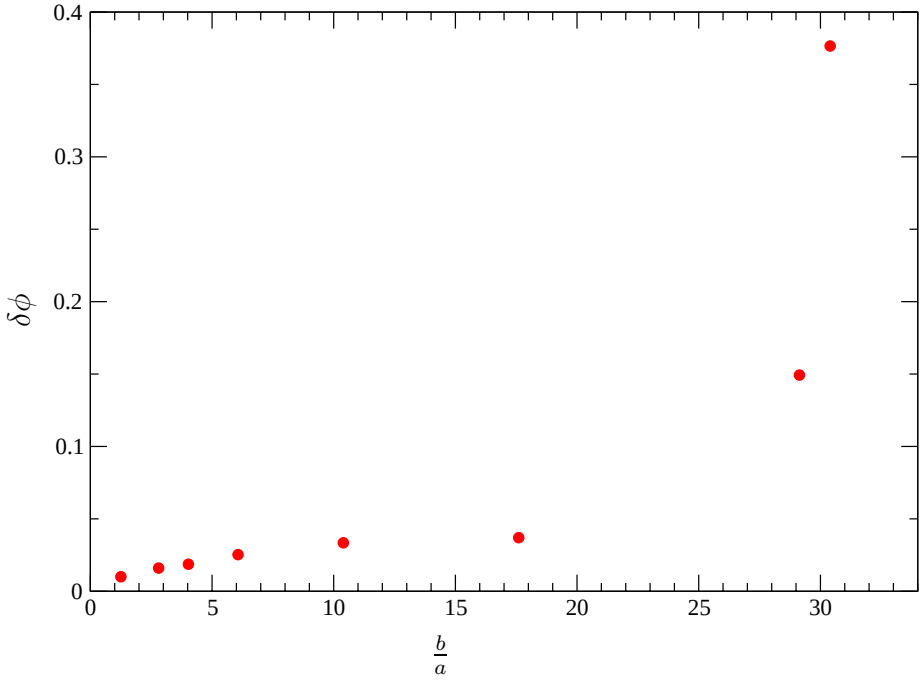

Figure 4.3: Depth of the dip in monomer density profile as a function of chain stiffness of the semiflexible polymers.

Further, the intrinsic width keep on increasing until we consider the flexible-semiflexible interface such that semiflexible polymers are isotropic. But the intrinsic width has smallest value for isotropic-nematic interface (i.e. the interface between flexible-stiff rod polymers). Therefore, the intrinsic width also decreases when we pass from isotropic-isotropic interface to isotropic-nematic interface of polymers i.e. intrinsic width decreases with increasing statistical segment length of semiflexible component when the statistical segment length is greater than the value at which isotropic-nematic transition takes place. In figure 4.4, it can be seen that the difference in total interfacial width and intrinsic width decreases as a function of statistical segment length of semiflexible component. This means the contribution from the capillary wave to the interfacial width also de-

creases as a function of statistical segment length of semiflexible component. In all these

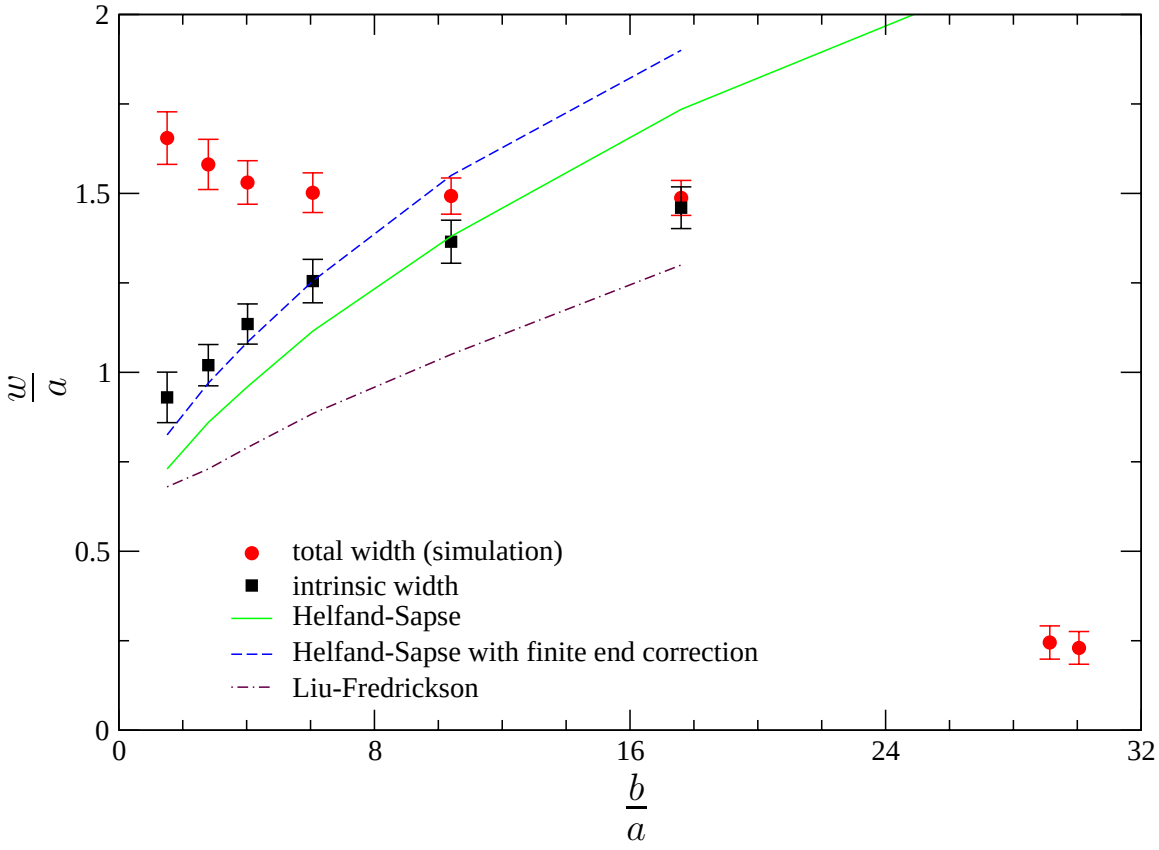

Figure 4.4: Interfacial width as a function of statistical segment length of semiflexible polymers. The width and statistical segment length both are in units of average bond length.

Within the work shortly characterized above Helfand and Sapse [20] obtained for the intrinsic interfacial width parameter w,

$$w = \sqrt{\frac{\beta_A^2 + \beta_B^2}{2\alpha}} \tag{4.7}$$

The results for our systems are again obtained with the replacements according to Eqs. 4.4 and 4.2 and shown also in Fig. 4.4. The end effect rises the value of interfacial width by a factor of $(1+\frac{2\ln 2}{\chi N})$ [89]. Figure 4.4 also presents the data obtained by using this correction factor in the mean-field expression obtained by Halfand-Sapse i.e Eq. 4.7. As for the interfacial tension a reasonable agreement between the intrinsic width and mean-field data with finite end corrections is observed in the semiflexible range and

increasing differences approaching the isotropic-nematic transition. The intrinsic width approaches the total width for large stiffness disparities because the increasing interface stiffness prevents the formation of capillary waves within the considered subsystems.

Liu and Fredrickson [67] obtained for their wormlike chain model

$$w = \frac{\sqrt{2}}{3} a_0 \sqrt{\frac{\kappa_A + \kappa_B}{\chi}} \tag{4.8}$$

With the same treatment as for the interfacial tension the values for our systems are also shown in Fig. 4.4 and a similar relationship between the analytic results in [20] and [67] and our simulation data as in Fig. 4.1 can be observed for the predicted interfacial width.

Moreover, it should be noted that the results for the interfacial tension and the interface width derived in [38] from the Helfand and Sapse [20] results and also the results following from the free-energy-functional in [87] by minimization with the ínterface profile Eq. 3.28 and using the same mapping procedure as in Eqs. 3.4 and 4.3 agree completely with the results in Figs. 4.1 and 4.4 for the case $C_{\infty A} = C_{\infty B} = 1$ but show strong increasing deviations at larger stiffness disparities. Using instead Eqs. 3.4 the formal equivalent mapping procedure

$$\begin{aligned} b' &= a\sqrt{C_{1N}} \\ \chi'_b &= \chi \\ \rho'_b &= \rho_0 \end{aligned} \tag{4.9}$$

leading also to Eq. 4.5 but now with parameters b' , χ'_b and ρ'_b , an almost complete agreement with the analytic results in Figs. 4.1 and 4.4 up to large stiffness disparities is obtained.

Mueller and Werner [38] have also reported that the total interfacial width decreases with increase in the stiffness of semiflexible component in the blend of flexible-semiflexible polymers which agrees with the present results.

4.2.3 Orientation of Chains and Bonds in the Interface Region

The thermodynamic quantities which were discussed in previous subsections are not sufficient to understand the microscopic structure of the polymer interfaces. The width of the interfacial region and the orientation of polymers on different length scales influence the material properties. They also play an important role for reactions at interfaces. The polymers stretch parallel to the interface. The shape of a polymer, near the interface is a prolate ellipsoid. The existence of a planar interface destroys the isotropy in the bulk polymer and consequently orientation of bonds as well as chains relatively to the interface will be observed.

Quantitatively, the orientation of the bond vectors near the interface region have been studied. We study the following bond orientational parameter (defined in the chapter 3);

$$S(x) = \frac{3\langle a_x^2(x)\rangle / \langle a^2\rangle - 1}{2} \tag{4.10}$$

where $\vec{a}$ are the bond vectors. The bond orientation parameter is positive for perpendicular and negative for the parallel orientation. The profile of the bond orientation is shown in the figure 4.5. In figure it is seen that bond vectors prefer to allign parallel to the interface. The orientation effects increases upon increasing the stiffness of the semiflexible component. Further the bond orientation parameter are not much different for different systems of studies in the flexible side whereas in the semiflexible side they are different which is the effect of stiffness of the semiflexible component. In the orientational profile the oriented region is broader in the compartment occupied by the stiffer chains. Further, in contrast to the width of the density profile, the spatial range over which the orientation of bonds extends grows with increase in the stiffness of the semiflexible component. Therefore, the orientational width and the width of the compositional profile are two independent microscopic length scales. Similar results are obtained by Mueller and Werner [38].

Further, we have studied the orientation of the parallel and the perpendicular components of the radius of gyration of the polymer chains. We have studied the following orientational parameter (as defined in the chapter 3) for the polymer chains near the interface;

$$\Delta Rg_{\perp} = \frac{3 < Rg_x^2 > - < Rg^2 >}{2 < Rg^2 >} \tag{4.11}$$

and

$$\Delta Rg_{\parallel} = \frac{3(< Rg_z^2 > + < Rg_y^2 >)/2 - < Rg >^2}{2 < Rg^2 >} \tag{4.12}$$

where $\Delta Rg_{\perp}$ and $\Delta Rg_{\parallel}$ are the perpendicular and parallel orientational parameters of the radius of gyration of polymer chains (perpendicular and parallel with respect to the interface plane), $< Rg^2 >$ is the mean squared radius of gyration of the chains and $< Rg_i^2 >$ $(i = x, y, z)$ is the ith component of mean squared radius of gyration of the polymer chains. Therefore, if the chains orient parallel to the interface, parallel orientational parameter ($\Delta Rg_{\parallel}$) will be positive (maximum value 0.25) while the perpendicular orientational parameter ($\Delta Rg_{\perp}$) will be negative (minimum value -0.5). If the chains orient perpendicular to the interface, $\Delta Rg_{\parallel}$ will be negative and $\Delta Rg_{\perp}$ will be positive. If there is no preferred orientation of the chains, $\Delta Rg_{\parallel}$ and $\Delta Rg_{\perp}$ both the quantities will be equal to zero. The profiles of these quantities are shown in the figure 4.6.

As shown in the figure, $\Delta Rg_{\parallel}$ and $\Delta Rg_{\perp}$ in the flexible side remains almost constant (until the persistence length ($\frac{l_p}{a}$) of the semiflexible chains increases upto 13.6) while in the semiflexible side they are different which is not unexpected as semiflexible chains

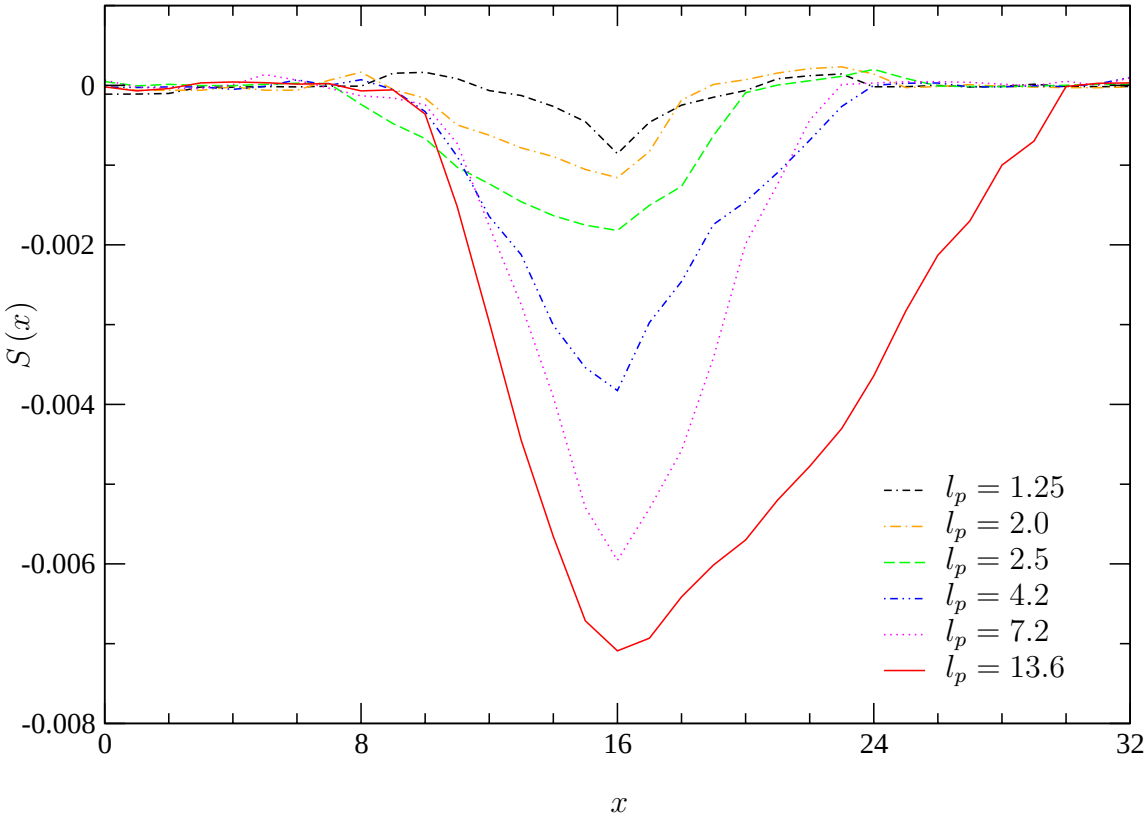

Figure 4.5: Orientation parameters of bonds as a function of stiffness of semiflexible component. l_ps are in unit of average bond length.

possess different degrees of flexibilities. In the isotropic-nematic interface, the chains in the flexible side remains unaffected till they are very close to interface. However, at the vicinity of the interface, they strongly stretch parallel to the interface. At the mean time, in the semiflexible region the semiflexible chains get stretched more and more parallel to the interface as the degree of flexibility decreases. In the isotropic-nematic interface the nematic chains prefer to allign parallel to the interface and they do it perfectly which is depicted in the figure 4.6. The polymer chains prefer to allign parallel to the interface as $\Delta Rg_{\parallel}$ is positive in all the cases and $\Delta Rg_{\perp}$ is negative (at the interface region) while in both bulk phases no preferential orientation takes place for the isotropic-isotropic interface. In the case of isotropic-nematic interface, nematic chains prefer to allign perfectly parallel to the interface plane even in the bulk phase. The orientation effects become stronger with the increase of the stiffness of semiflexible chains. For isotropic -isotropic interfaces, the orientational effect tends to be small unless the system is close to the isotropic-nematic transition. Passing through the interface region the elliptic chains first attempt to maximize the homocontacts with their own bulk phase (A-A and B-B segment contacts, respectively) in order to minimize the energy by rotating their longest axes into the interface plane as far as possible.

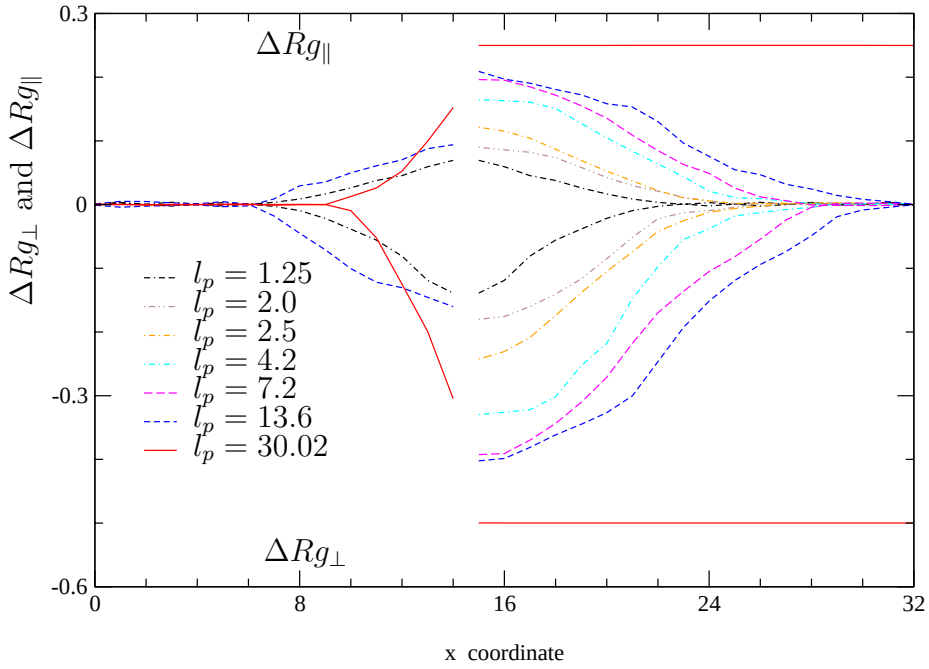

Figure 4.6: Orientation parameters of chains as a function of stiffness of semiflexible polymers. The persistence length are in units of average bond length.

4.2.4 Distribution of the Chain Ends and Density of Center of Mass of the Chains

The distribution of the chain ends are important for the interdiffusion and healing properties at interfaces between long polymers [15]. Further on the theoretical side, the behavior of chain ends is related to corrections to the ground state approximations [90]. Chain end effects give a large corrections to the interfacial tension and width (e.g., see the subsections 4.2.1 and 4.2.2) and they also play an important role for long range interactions between interfaces. Due to entropic reason polymers orient themselves by putting their ends preferentially at the center of the interfaces. Since A type of chains (in polymer blend of type A and type B) close to the interface prefer to put the chain ends into the B phase and vice versa, the chain ends are more at the interface than they are at the bulk side. A chain close to interface prefers to put its ends to its minority phase because of entropic reason. Therefore the density of ends of type A chains is increased at the side of type B chains and decrease close to the interface at the A side and vice versa. When this effect increases the interface becomes sharper and we cannot see such a effect in the weak segregation limit. If we calculate the total chain end distributions, we find effectively an enrichment of chain ends at the center of the interface and a depletion in the wings of the profile. The result of polymer chain ends being located preferentially

close to the interface is that whole chains tend to orient themselves parallel to the interface and hence the shape of the polymer chains near the interface is prolate ellipsoid (see previous su

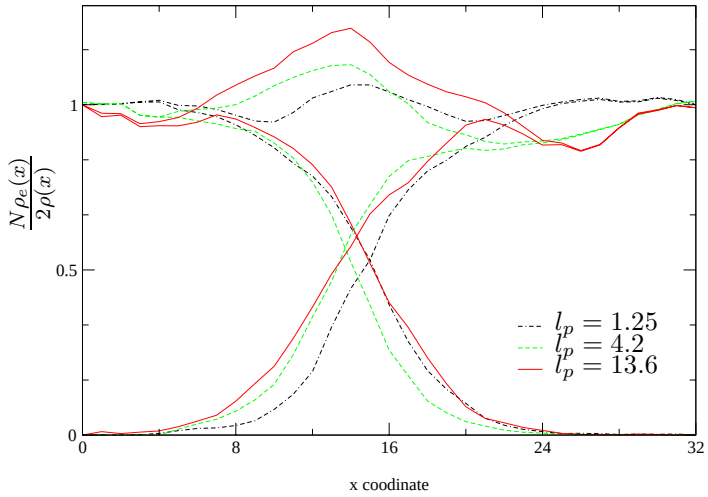

Figure 4.7: Distribution of chain ends as a function of stiffness of semiflexible components in flexible-semiflexible polymer systems. The persistence lengths l_ps are in units of average bond length.

Figure 4.7 shows the profiles of the distribution of the chain ends as a function of stiffness of semiflexible components. In Fig. 4.7, $\frac{N\rho_e(x)}{2\rho(x)}$ versus x coordinate haven been plotted where $\rho_e(x)$ is the number density of chain ends at 'x', $\rho(x)$ is the total monomer density at 'x' and N is the number of monomer per chain. We have presented the above described quantitiy as a function of chain stiffnes of semiflexible component. It shows the chain end distributions for flexible chains, semiflexible chains and sum of them. Chain ends are enriched at the center of the interface, and this effect goes along with a depletion away from the interface. A - polymers like to put their ends into B rich phase and vice versa. Similar results are obtained theoretically for Gaussian chains by Schmid and Mueller [66]. The effect becomes stronger when the chain stiffness increases. In the figure 4.7, it can be seen that the maximum value of the profile increases with the increase of the stiffness of semiflexible component of the blend. As a result the minimum value away from the interface is smallest for the system having highest value of stiffness for semiflexible component. Further the total chain end distribution becomes more asymmetric as a function of stiffness of semiflexible component. In the flexible side the profiles are not much different but in the semiflexible side they are different which is reflected at the total value of end distributions.

Analogous observations apply to figure 4.8 which presents the normalized density of centers of mass of the chains, $\frac{\rho_{cm}(x)}{\rho_{cm}}$ (where $\rho_{cm}(x)$ is the number density of center of mass of polymer chains at x and ρ_{cm} is the average density of center od mass of polymer

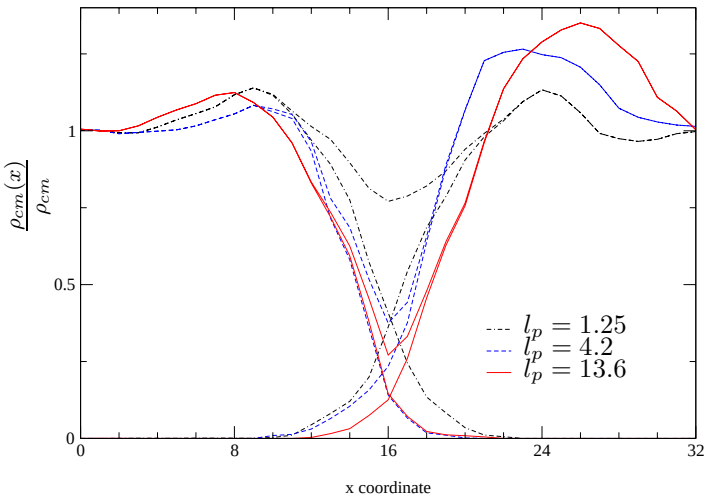

Figure 4.8: Distribution of center of mass of flexible chains, semiflexible chains and sum of them. The persistence lengths l_ps are in units of average bond length.

chains) except for the maxima at the interface being now exchanged to minima due to the enrichment of centers of mass of chains in the interface region next to the bulk phase of the component. The density of center of mass has a minima at the center of the interface. This figure presents the normalized density of center of mass of flexible chains, semiflexible chains and the sum of them. The profile has minimum at the interface and this effect goes on increasing as the stiffness of the semiflexible component increases while the maxima at the interface in the profile of the chain ends distribution goes on increasing with the increase in the stiffness of the semiflexible component. As in the case of chain end distributions, the profiles in the flexible side are not much different but in the semiflexible side they are. Therefore, the total profiles are not symmetric. The maximum value in the profile which contains sum of center of mass of flexible and semiflexible chains away from interface increases as a function of stiffness of semiflexible component.

4.3 Interfaces of Polymers Having Different Monomer Sizes

In the previous section the results of interface properties of flexible-semiflexible polymer systems are discussed. This section is devoted to results and discussions about the interface properties of polymers with different monomer sizes. These systems consist of two types of polymer chains, viz; type A and type B. A type of polymer chains have monomers with diameter $d_A = d_{min}$ (which is defined already in chapter 3) whereas B type of polymer chains have monomers with diameter, $d_B = 2 \times d_A$. We study and compare interfacial properties of polymers having monomers of different sizes 'monomer size disparity with equal number of monomers per chain' and 'monomer size disparity with

almost equal radius of gyration' (see chapter 3). The interface properties of monomer size disparity systems are compared to that of symmetrical system.

The interfacial properties which have been studied, are as those of stiffness disparity presented in section 4.2. The interfacial properties namely, interfacial tension, interfacial width, density profile, orientation of chains, distribution of chain ends and center of mass of chains for the systems described above have been studied.

4.3.1 Interfacial Tension

The interfacial tension for unsymmetric systems of two types of polymers which differ in the sizes of monomers are calculated as described above by virial theorem and these results are compared with the analytic expression given by Helfand and Sapse [20];

$$\frac{\sigma}{k_B T} = \frac{2}{3}\sqrt{\alpha}\left(\frac{(\beta_A^3 - \beta_B^3)}{(\beta_A^2 - \beta_B^2)}\right) \tag{4.13}$$

which is same as in Eq. 4.1. The β_i ($i = A,\ B$) are same as in equation 4.2 and ρ_{0i} are also same as in equation 4.3 in the section 4.2. However, the interaction parameter, α, between two statistical segments is now given by,

$$\alpha = \chi\sqrt{\rho_A \rho_B} \tag{4.14}$$

with the Flory-Huggins parameter χ for the interaction of two beads of chains of different types as defined in equation 3.13. The mapping procedures to compare simulation results with mean field are same as in the subsection 4.2.1. From equation 4.1 it is seen that the interfacial tension depends mainly on number density of different components, the interaction parameter χ and statistical segment length of the two components.

Table 4.1 shows simulation results and the data obtained from mean-field expression of Helfand and Sapse equation (4.13). From table 4.1, it can be seen that the interfacial tension decreses with the increase in 'monomer size disparity'. It is seen that the interfacial tension decreases in both cases, namely in monomer size disparity with equal number of monomers per chain and monomer size disparity with almost equal radius of gyration, in comparison to symmetrical system containing smaller size of beads. Moreover, for the asymmetric systems the interfacial tension is higher for the monomer size disparity with almost equal radius of gyration than that for the monomer size disparity with equal number of monomers per chain. We have compared also the ratio of interfacial tension to the Flory-Huggins parameter, χ, for different systems of studies. Table 4.1 presents the ratio of $\frac{\sigma}{k_B T}$ and χ for the systems of study. The ratio of interfacial tension ($\frac{\sigma}{k_B T}$) to Flory-Huggins parameter, χ also has larger value for the monomer size disparity with almost equal size of polymer chains than that of monomer size disparity with equal number of monomers per chain.

It is clear that simulation data agrees very well with the mean-field data by taking into account the finite chain length effects. Following the description in subsection 4.2.1

type of system	$\frac{\sigma}{k_BT}$	$\frac{\sigma/k_BT}{\chi}$	$\frac{\sigma}{k_BT}$ H-S	$\frac{w}{a}$	$\frac{w}{a}$ (H-S)
symmetrical	0.0615 ± 0.0058	0.192	0.0707	1.655	0.73
$N_A = N_B$	0.0261 ± 0.007	0.133	0.0284	1.05	0.723
$R_g^A \sim R_g^B$	0.0303 ± 0.0075	0.143	0.0331	0.979	0.659

Table 4.1: Interfacial tension and width for size disparity systems and symmetrical system. The total interfacial width are divided by respective bond lengths that is, 1.998 in symmetrical system and 3.749 in the unsymmetrical systems.

we take into account of finite length effects to describe the small difference between simulation and mean field results. Helfand *et al.* [88] have obtained the corrections in the interfacial tension due to the finite length of the chains. They have obtained that the interfacial tension is reduced by a factor of $(1 - (\frac{\ln 2}{\chi N_A} + \frac{\ln 2}{\chi N_B})$ because of finite chain length of the polymer chains. This factor becomes ~ 0.8 for unsymmetric systems and describes very well the very small difference between simulation results and mean-field data obtained from the analytic expression of Helfand and Sapse. When the statistical segment length of one of the components increases i.e., when the asymmetry in two types of chains increases, the interfacial tension increases but in our system of study it decreases because the Flory-Huggins parameter and number density of the type B chains also decrease. From table 4.1, it is seen that the interfacial tension for the asymmetric system is lower than that for the symmetric system. As seen in the table 4.1 for the size disparity case simulation data agree very well with the mean field results which implies that the mean field results describe the systems of lower values of χ and number density. The main resons for the lower value of interfacial tension for asymmetric systems are the lower value of χ and monomer density. As seen from the Eq. 4.5 the interfacial tension depends up on both of these quantities and increase with the increase with any of these quantities. It is seen that the small increase in interfacial tension due to increase in statistical segment length of the asymmetric system cannot compensate the huge reduction due to number density and χ.

4.3.2 Density Profile and Interfacial Width

Figure 4.9 shows the normalized monomer density profile for the type A monomers type B monomers and their sum. The number density of type B monomers is multiplied by eight as one type B bead has volume 8 times larger than that of the type A in monomer size disparity systems. As in the case of stiffness disparity, one can describe these profiles by the tangent hyperbolic function, Eq. 3.28. A reduction of the total monomer density is observed at the center of the interface. It can be seen from figure that the monomer density profile for asymmetric polymer-polymer interfaces are not significantly different than that of the symmetric interfaces. In the case of asymmetric system the smaller beads penetrate more deep inside the bulk phase of larger beads than in the symmetrical system increasing the size of the interfacial region. The dip in the center of the interface increases slightly with monomer size disparity. But this increase is not

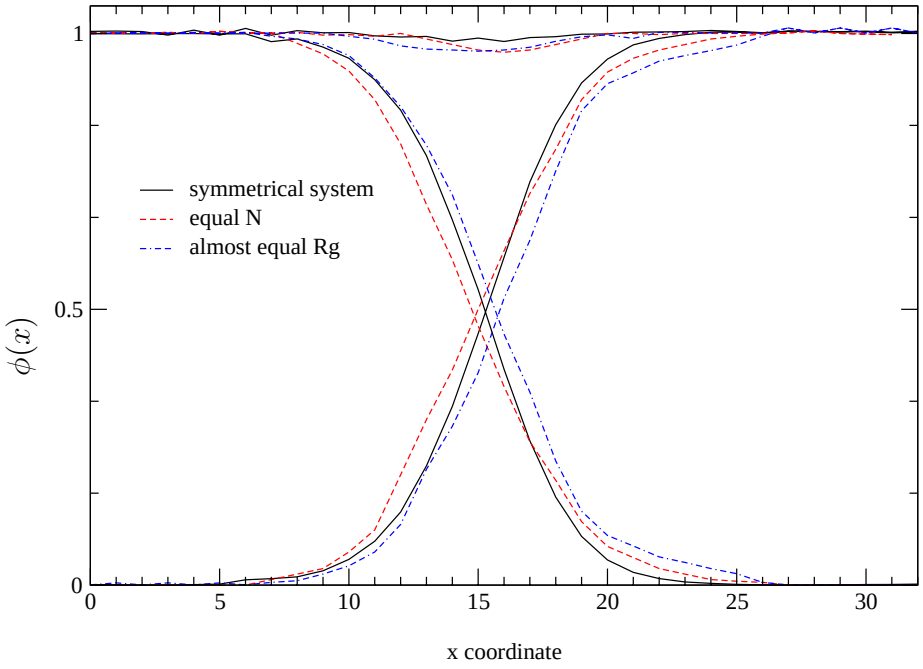

Figure 4.9: Monomer density profile of individual components and sum of them in the symmetric system and monomer size disparity systems.

significant as in the case of isotropic-nematic interface (see subsection 4.2.2). The dip at the center of the interface is highest for the system of monomer size disparity with equal number of monomers per chain for both types of chains whereas it has lowest value for the symmetric system.

Table 4.1 shows total interfacial width as a function of diameters of different types of beads. It depicted both the data one by simulation, and another by mean field expression using Eq. 4.7. The same mapping as in the stiffness disparity case has been used. These data show that total interfacial width increases with the asymmetry in the monomer volume, i.e., the radius of monomers. The interfacial width is larger for the system in which two types of monomers have differnt size but there are equal number of monomers per chain than that the system in which two different types of monomers have almost equal radius of gyration.

4.3.3 Orientations of Chains

In polymer blends the orientation of the polymers on different length scales influence the materials properties. The thermodynamic propterties like interfacial tensions are not enough to understand the microscopic structure of the polymer interfaces. The shape of a polymer chain is a prolate ellipsoid near the interface. Due to entropic reasons polymers orient themselves by putting their ends preferentially at the center of the

interface. In the present work, the orientation of chains have been studied by defining orientation parameter in terms of radius of gyration of polymer chains. The orientational profiles of monomer size disparity systems are compared with that of symmetric system. Orientations of the perpendicular and parallel (perpendicular and parallel with respect to interface) components of radius of gyration are studied. The orientational parameters which are studied are same as in the case of stiffness disparity Eq. 4.11 and 4.12. The orientational profiles are shown in the figure 4.10. The figure shows that the polymers in asymmetric systems with larger radius of beads orient more parallel to the interface plane compared to symmetrical systems. Further the effect is less for the system of the monomer size disparity with almost equal radius of gyration of chains than the system of the monomer size disparity with equal number of monomers per chain. Mostnotably, the orientation parameter in the side of small beads are not much different. If we see only A types of chains (chains with small beads, i.e. left side in the figure 4.10), they stretch more in the asymmetric system than that in the symmetric system. It is seen that A types of chains are not much influenced by the interface and B types of chains get more affected by the interface. Generally, there is weak nematic ordering near the interface but it is seen from our results that the effect is stronger in asymmetric system with smaller and larger beads than the symmetric system with the smaller beads. Passing through the interface region the elliptic chains first attempt to maximize the homocontacts with their own bulk phase (A-A and B-B segment contacts, respectively) in order to minimize the energy by rotating their longest axes into the interface plane as far as possible.

4.3.4 Distribution of the Chain Ends and Density of Center of Mass of the Chains

Since A types of chains (in polymer blend of type A and type B chains) close to the interface prefer to put the chain ends into the B phase and vice versa, the chain ends are more at the interface than they are at the bulk side. A chain close to interface prefers to put its ends to its minority phase because of entropic reason. Therefore the density of ends of type A chains is increased at the side of type B chains and decrease close to the interface at the A side and vice versa. When this effect increases the interface becomes sharper and we cannot see such a effect in the weak segregation limit. If we calculate the total chain end distributions, we find effectively an enrichment of chain ends at the center of the interface and a depletion in the wings of the profile. As a result whole chains tend to orient themselves parallel to the interface and hence the shape of the polymer chains near the interface is prolate ellipsoid (see above).

Figure 4.11 shows the distribution of the chain ends. Here we have plotted $\frac{N\rho_e(x)}{2\rho(x)}$ versus x coordinate where $\rho_e(x)$ is the number density of chain ends, $\rho(x)$ is the total monomer density and N is the number of monomers per chain. Here we have presented described quantity as a function of monomer size disparity in our systems of study. Figure shows the chain end distributions for type A chains (i. e. chains having small size of beads), for type B chains (i.e. beads with large size of beads) and sum of them. Fur-

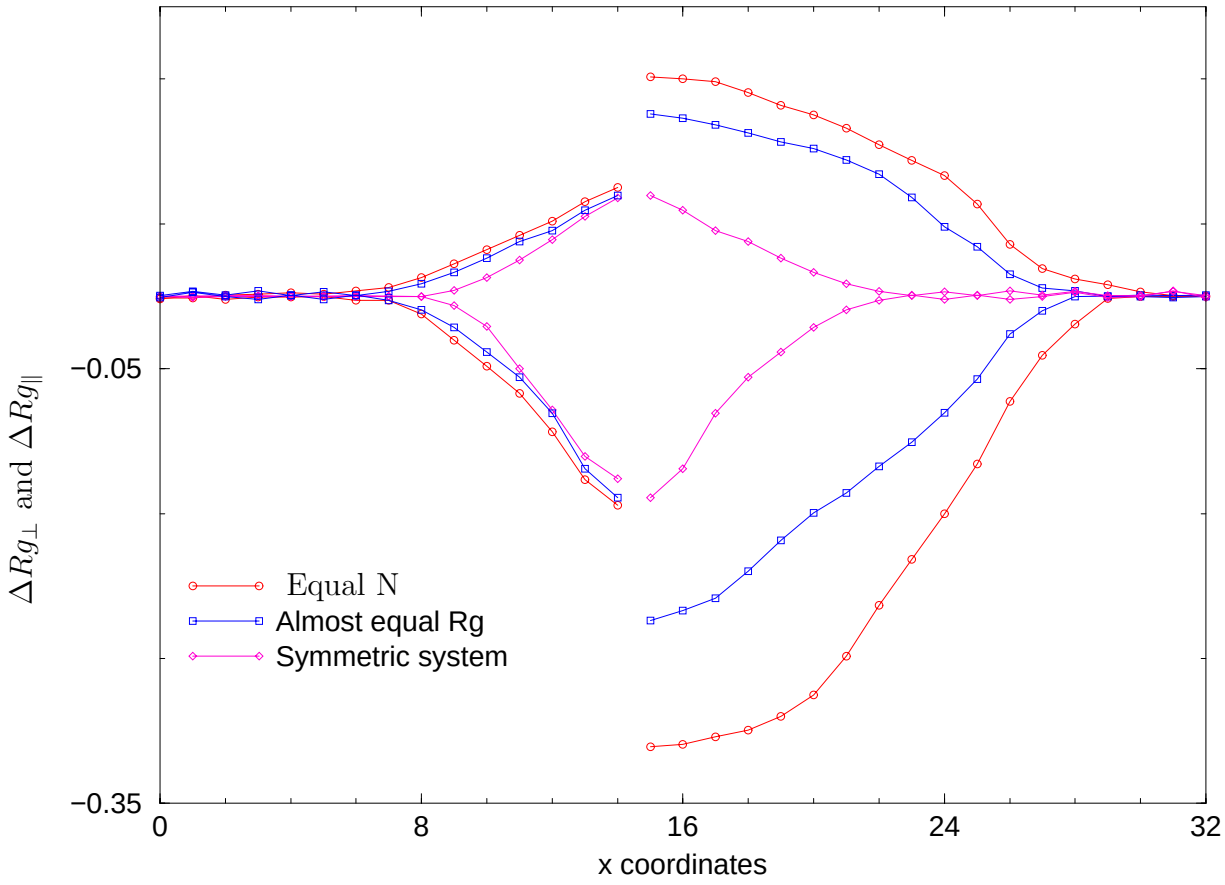

Figure 4.10: Orientation of chains in the symmetric system and monomer size disparity systems.

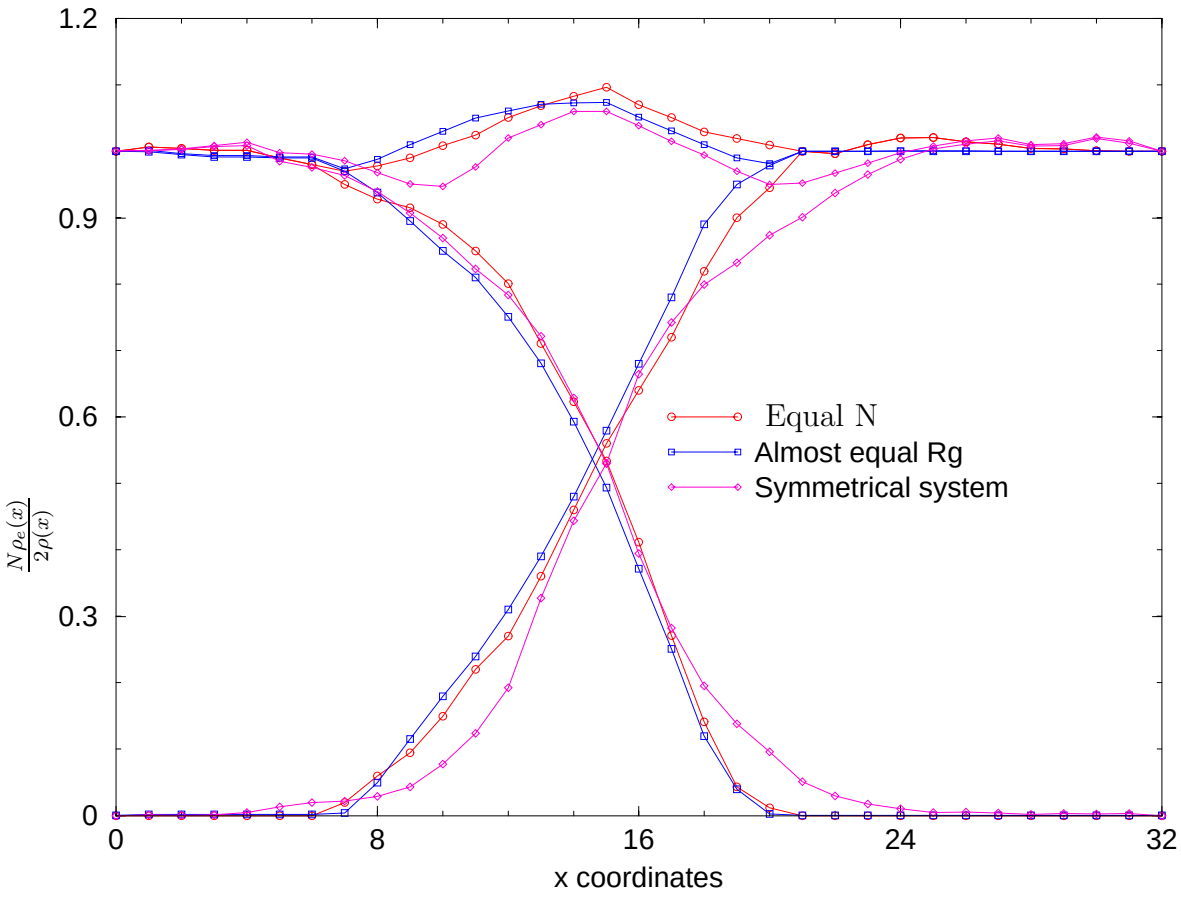

Figure 4.11: Distribution of chain ends in symmetric systems and in systems with different monomer sizes.

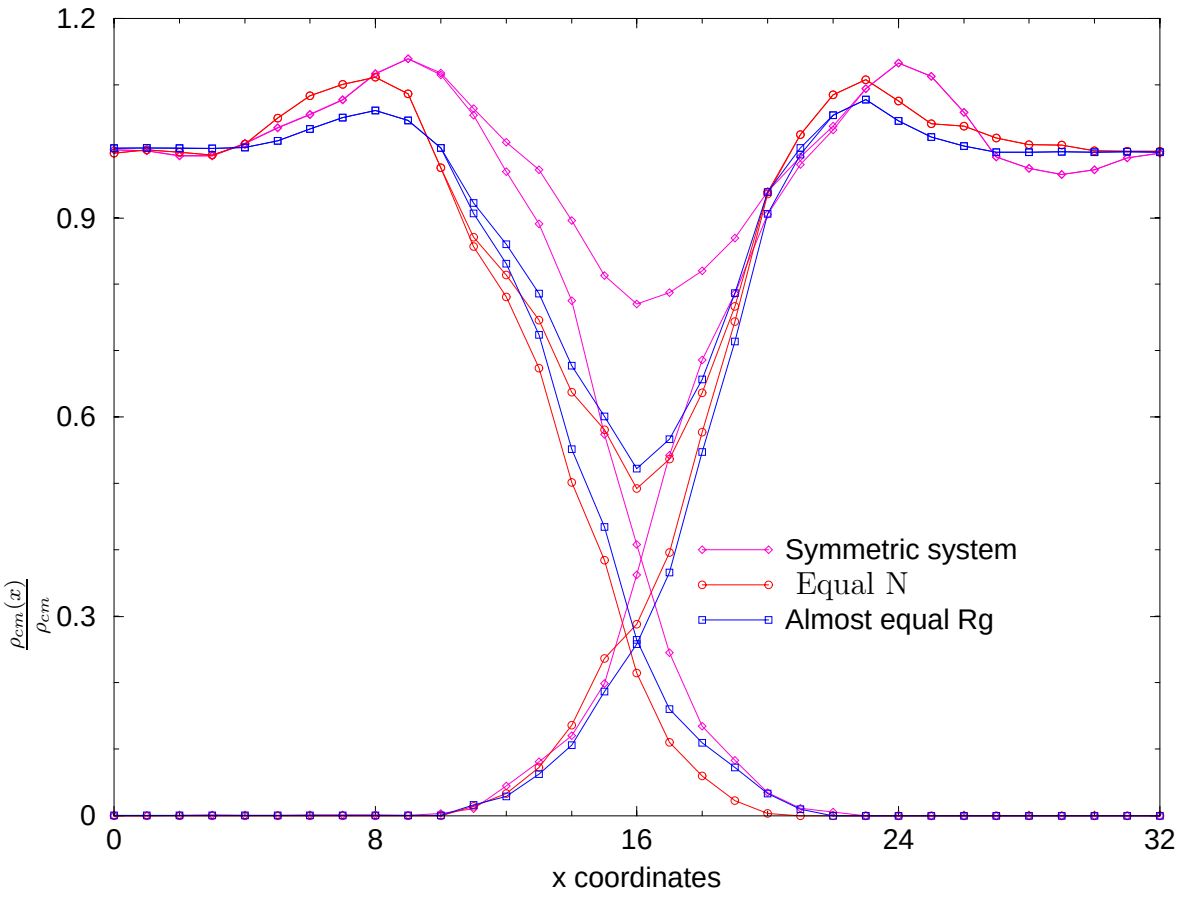

Figure 4.12: Distribution of center of mass of chains in symmetric system and systems with different monomer sizes.

ther, it depicted chain end distribution for symmetrical system. It is seen that the chain ends are enriched at the center of the interface. The effect increases with the monomer size disparity. The peak has highest value for asymmetric system such that larger bead size component has equal number of monomers per chain as that of chains with smaller beads whereas the peak has lowest value for the symmetrical system. Total chain end distribution becomes asymmetric for the asymmetric systems which we studied.

The distribution of the center of mass of chains are also important to understand the interfacial properties as they give us insight of the location of chains. The profile for the distribution of chain center of mass, viz; $\frac{\rho_{cm}(x)}{\rho_{cm}}$, is shown in figure 4.12. $\rho_{cm}(x)$ is the density of center of mass of polymer chains at x and ρ_{cm} is the average density of center of mass of chains. Therefore, this figure presents the normalized density of centers of mass of the chains. In the chain end distributions, there is a maxima at the center of interface (in total chain end distribution) whereas the total density of center of mass has minima at the center of interface. In figure 4.12 we have presented the normalized density of center of mass for type A chains (i.e. chains having smaller beads), for type B chains (i.e. chains having larger beads) and sum of them. Further, to compare the results of asymmetric systems to that of symmetrical system, we have presented distribution of center of mass for the symmetrical system also. The minimum value at the center of interface is lowest for asymmetrical system in which both types of chains have equal number of monomers per chain and it is highest for the symmetrical system.

4.4 Phase Behavior in Flexible-Semiflexible Polymer Blend

We study the dependence of critical value of Flory-Hugins parameter, χ, and hence the critical temperature T_c on stiffness of semiflexible component.

In this section, the critical value of $\chi(\chi_c)$ has been estimated as a function of stiffness of semiflexible components in flexible-semiflexible polymer blend. As described in chapter 2, one can study phase diagram in polymeric systems by using semi-grandcanonical ensemble. In this method one types of chains are converted into other type and vice versa, to take into account density fluctuation. The total number of particles in the system remains constant. However, we consider very high stiffness disparity, so this method becomes inefficient as it violates excluded volume effect. The behavior of interfacial tension and interfacial width in weak segregation limit has been studied and from these data critical value of χ has been estimeted. In the present work, we estimate value of χ at which interfacial tension vanishes by studying behavior of interfacial tension at weak segregation limit. The behavior of interfacial tension at strong segregation limit will be also discussed.

To know whether the system has attained equilibrium in the weak segregation limit,

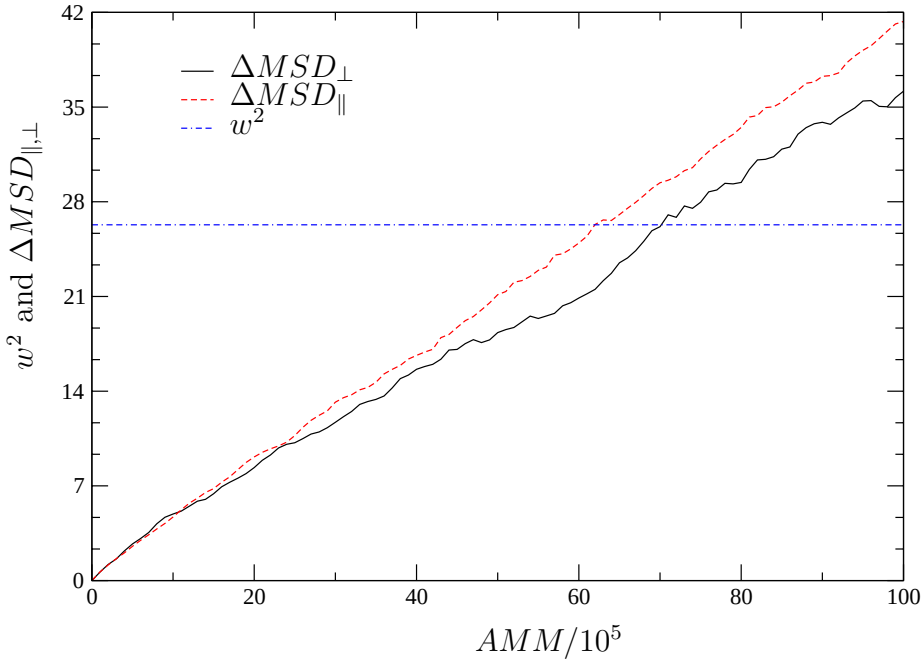

Figure 4.13: MSD of center of mass of polymers and square of interfacial width versus the AMM for weak segregation limit for flexible-semiflexible system in which semiflexible polymers have persistence length $(\frac{l_p}{a})$ =4.2 when χ =0.136.

the interfacial width and the mean squared displacement (ΔMSD) of center of mass are monitored. For the weak segregation limit the interfacial width increases (see below) and hence the idea which was used for the strong segragation limit (see section 3.2.2) may not be enough for the equilibration. If the square of interfacial width and ΔMSD are comparable, the calculations of interfacial tensions and interfacial widths are started. Figure 4.13 shows the graph ofΔMSD and square of width for persistence length $(\frac{l_p}{a})$= 4.2. In all the systems of weak segregation limit, such graphs are produced before starting any calculations to ensure the system has attained equilibrium condition.

4.4.1 Interfacial Tension in Strong and Weak Segregation Limit

In the strong segregation limit, mean-field theory predicts that the interfacial tension varies as the square root of Flory-Huggins parameter, χ (Eq. 4.1) . However, in the weak segregation limit the behavior is different. In weak segregation limit Flory-Huggins-de Geenes formula for interfacial tension and interfacial width are given by (from chapter 2);

$$\frac{\sigma}{k_B T} = \frac{9}{b^2\sqrt{N}}\left(1 - \frac{\chi_c}{\chi}\right)^{3/2} \tag{4.15}$$

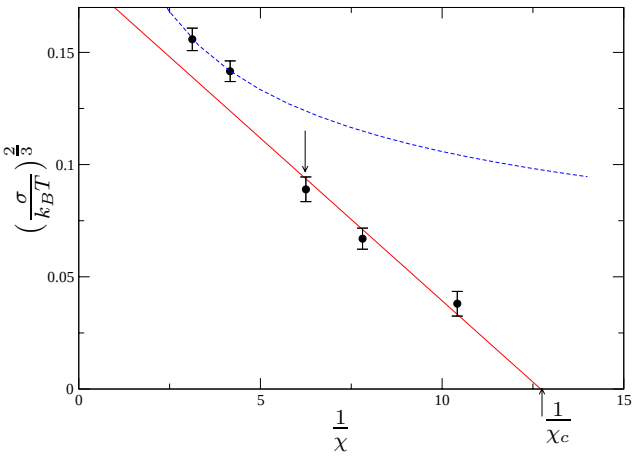

Figure 4.14: $(\frac{\sigma}{k_BT})^{\frac{2}{3}}$ versus $\frac{1}{\chi}$ in flexible-flexible polymer system. The solid line is the straight line fitted to the weak segregation data and dashed line is the curve from the formula of strong segregation limit (Eq. 4.1).

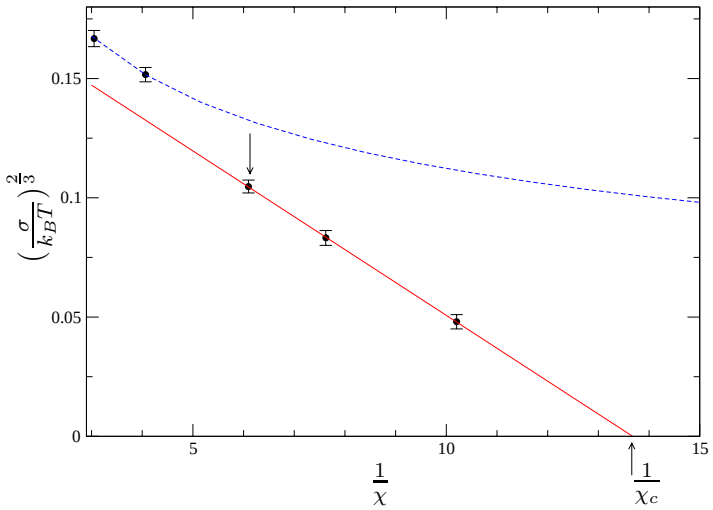

Figure 4.15: $(\frac{\sigma}{k_BT})^{\frac{2}{3}}$ versus $\frac{1}{\chi}$ in flexible-semiflexible polymer system in which semiflexible component has persistence length ($\frac{l_p}{a} = 2.0$). The solid line is the straight line fitted to the weak segregation data and dashed line is the curve from the formula of strong segregation limit (Eq. 4.1).

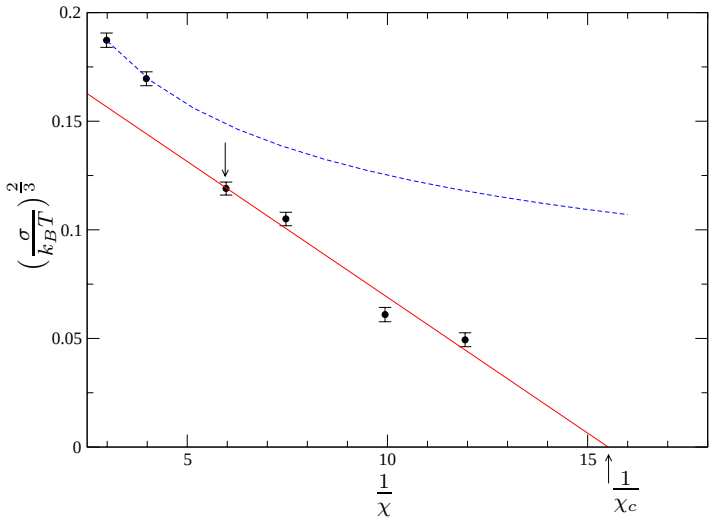

Figure 4.16: $(\frac{\sigma}{k_BT})^{\frac{2}{3}}$ versus $\frac{1}{\chi}$ in flexible-semiflexible polymer system in which semiflexible component has persistence length ($\frac{l_p}{a} = 2.5$). The solid line is the straight line fitted to the weak segregation data and dashed line is the curve from the formula of strong segregation limit (Eq. 4.1).

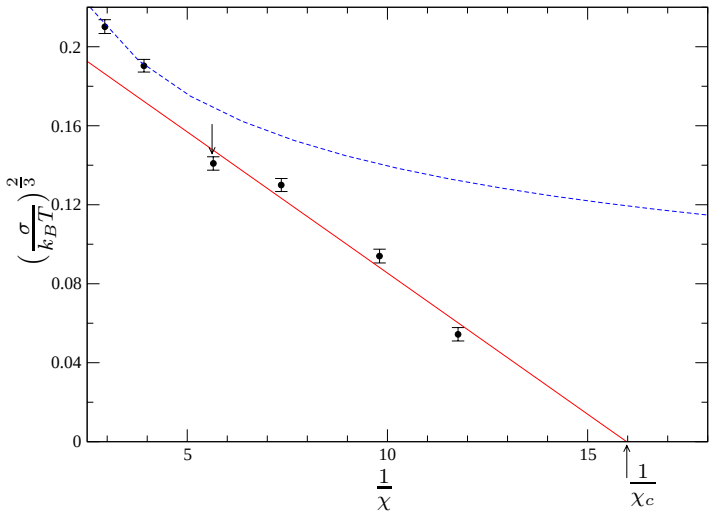

Figure 4.17: $(\frac{\sigma}{k_BT})^{\frac{2}{3}}$ versus $\frac{1}{\chi}$ in flexible-semiflexible polymer system in which semiflexible component has persistence length ($\frac{l_p}{a} = 4.2$). The solid line is the straight line fitted to the weak segregation data and dashed line is the curve from the formula of strong segregation limit (Eq. 4.1).

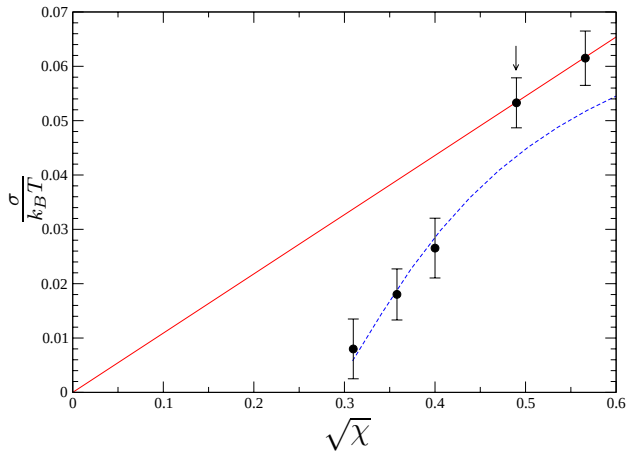

Figure 4.18: Interfacial tension versus $\sqrt{\chi}$ for flexible-flexible polymer system. The solid line is the straight line from the Eq. 4.1 and the dashed line is the curve from Eq. 4.15.

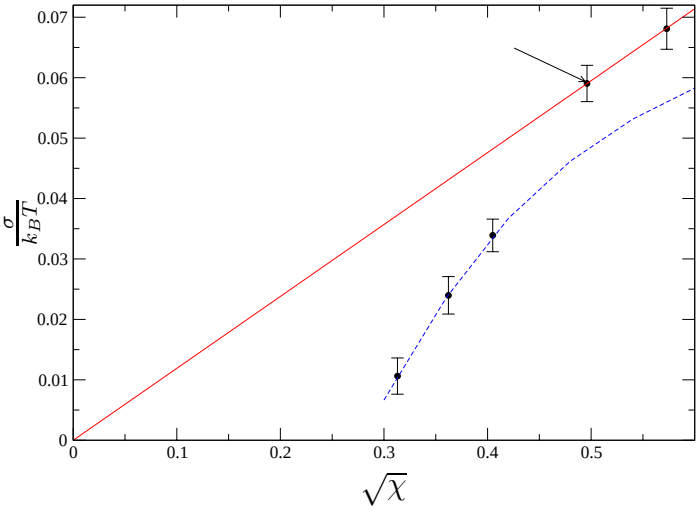

Figure 4.19: Interfacial tension versus $\sqrt{\chi}$ for flexible-semiflexible polymer system in which semiflexible component has persistence length ($\frac{l_p}{a} = 2.0$). The solid line is the straight line from the Eq. 4.1 and the dashed line is the curve from Eq. 4.15.

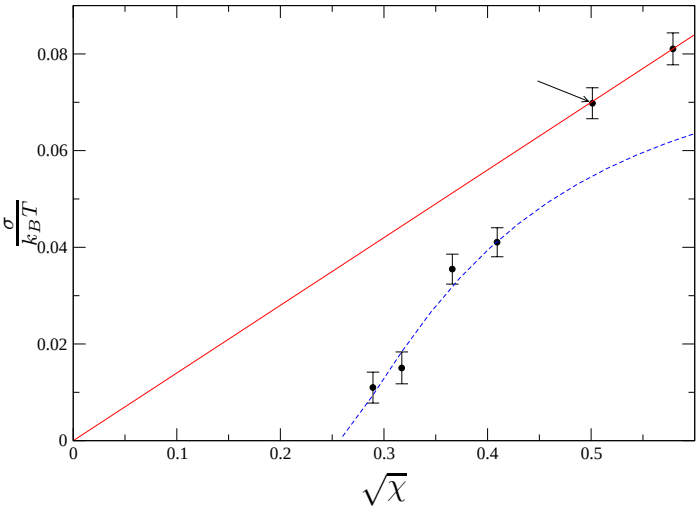

Figure 4.20: Interfacial tension versus $\sqrt{\chi}$ for flexible-semiflexible polymer system in which semiflexible component has persistence length ($\frac{l_p}{a} = 2.5$). The solid line is the straight line from the Eq. 4.1 and the dashed line is the curve from Eq. 4.15.

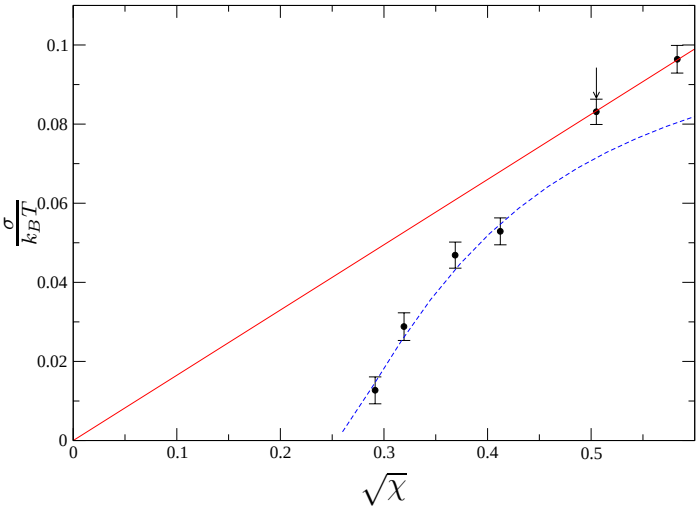

Figure 4.21: Interfacial tension versus $\sqrt{\chi}$ for flexible-semiflexible polymer system in which semiflexible component has persistence length ($\frac{l_p}{a} = 4.2$). The solid line is the straight line from the Eq. 4.1 and the dashed line is the curve from Eq. 4.15.

systems	Eq. 4.15	Eq. 4.1	Eq. 4.15 M-F	Eq. 4.1 M-F
l_p =1.25	0.18402	0.109	0.1744	0.125
l_p =2.0	0.1886	0.121	-	0.145
l_p =2.0	0.1939	0.14	-	0.165
l_p =4.2	0.2283	0.165	-	0.192

Table 4.2: Table of the prefactors in equations 4.15 and 4.1 obtained after comparing our data with mean filed. Here l_ps are in units of average bond length. In the column of system means, the system contains flexible polymers and semiflexible polymers of given persistence length.

and

$$w = \frac{b\sqrt{N}}{3}\left(\frac{\chi}{\chi_c} - 1\right)^{(-1/2)} \tag{4.16}$$

respectively. In these equations, b is statistical segment length, N is the number of monomers per chain and χ_c is the critical value of χ. To derive these formulas, it is assumed that the system is symmetrical, i.e. the number of monomers per chain in type A and type B polymers is equal and further the statistical segment length for both types of chains are equal. Therefore, when one considers asymmetrical systems the prefactors in equations 4.15 and 4.16 will be different. However, exponents in right hand side will be the same. From the equation 4.15, it is seen that interfacial tension decreases with decrasing χ and finally vanishes when $\chi = \chi_c$. Similarly, from 4.16 the interfacial width increases with decrasing χ and finally becomes infinite when $\chi = \chi_c$.

As described above (see Eq. 4.15), $(\frac{\sigma}{k_BT})^{\frac{2}{3}}$ linearly varies with $\frac{1}{\chi}$ and the interfacial tension vanishes when $\chi = \chi_c$. Figure 4.14 shows the dependence of $(\frac{\sigma}{k_BT})^{\frac{2}{3}}$ on $\frac{1}{\chi}$ for the flexible-flexible polymer system. We can describe the behavior by a straight line as shown. Further, the figure shows interfacial tension at strong segregation limit and described curve (see Eq. 4.1 and 4.5). It can be seen in the figure that the data of strong segregation limit (SSL) does not follow the straight line fitted for the data of weak segregation limit (WSL). From the fitted straight line for the data of interfacial tension in weak segregation limit, we have estimated the critical value of χ. Further, the prefactors in equation 4.15 also has been calculated. Table 4.2 shows the prefactors in the equation 4.15, from mean field and present work. The prefactors from mean-field and present work are not much different. The difference is less than 5%.

Figure 4.18 presents interfacial tension as a function of square root of χ for all the range of study in the present work for the flexible-flexible polymer system. From figure 4.18 it can be seen that the data of strong segregation limit follow a linear behavior whereas that of weak segregation limit shows different behavior. We have calculated the slope of the straight line described to the data at SSL which is not far from the mean-filed value. Table 4.2 shows the slope of the fitted line from present work and mean filed.

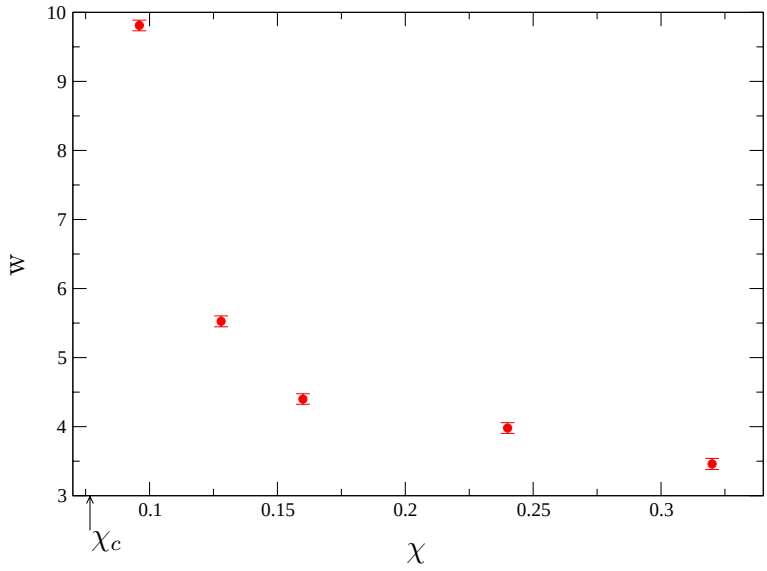

Figure 4.22: Total interfacial width as a function of the interaction parameter, χ for flexible and semiflexible with persistence length ($\frac{l_p}{a} = 1.25$). Arrow marks the critical value of χ, estimated using the data of interfacial tension.

Figures 4.15, 4.16 and 4.17 presents the interfacial tension in WSL for the system of flexible-semiflexible polymers in which semiflexible chains have persistence length ($\frac{l_p}{a}$) =2.0, 2.5 and 4.2 respectively. Also shown are the data for SSL. As described above, for the flexible-flexible polymer system, we have estimated the critical value of χ for all these systems of study and presented in figure 4.26. The prefactors in the equaion 4.15 are determined for all the systems of study and presented in the table 4.2. Figures 4.19, 4.20 and 4.21 presents the interfacial tension as a function of square root of χ for all the range of study in the present work for the system of flexible-semiflexible polymers in which semiflexible chains have persistence length ($\frac{l_p}{a}$) =2.0, 2.5 and 4.2 respectively. Further, table 4.2 presents the slope of the straight line fitted for SSL case.

4.4.2 Interfacial Width in Weak and Strong Segregation Limit

Figure 4.22 shows the dependence of total interfacial width on Flory-Huggins parameter, χ, for flexible-flexible polymer blend. In figure 4.22, the arrow marks the critical value of χ estimated from the interfacial tension. From figure, it can be seen that the interfacial width diverges at very very low value of χ. Werner and coworkers [81] also have studied the behavior of interfacial tension, width and other interfacial properties at weak segregation limit using Monte Carlo techniques. Similarly, other figures 4.22, 4.24 and 4.23 show the interfacial width as a function of χ for the system of flexible-semiflexible polymers in which semiflexible chains have persistence length ($\frac{l_p}{a}$)= 2.0, 2.5 and 4.2 respectively. It can be seen from the figures that the interfacial width increases

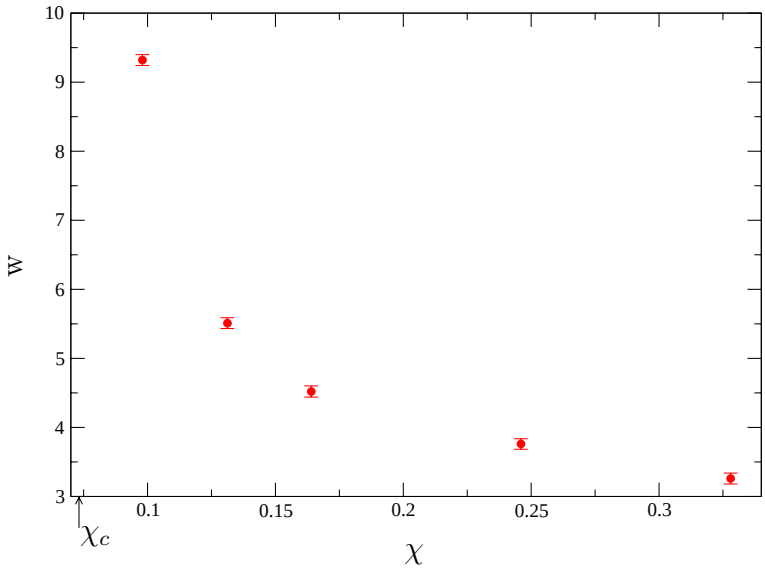

Figure 4.23: Total interfacial width as a function of the interaction parameter, χ for flexible and semiflexible with persistence length ($\frac{l_p}{a} = 2.0$). Arrow marks the critical value of χ, estimated using the data of interfacial tension.

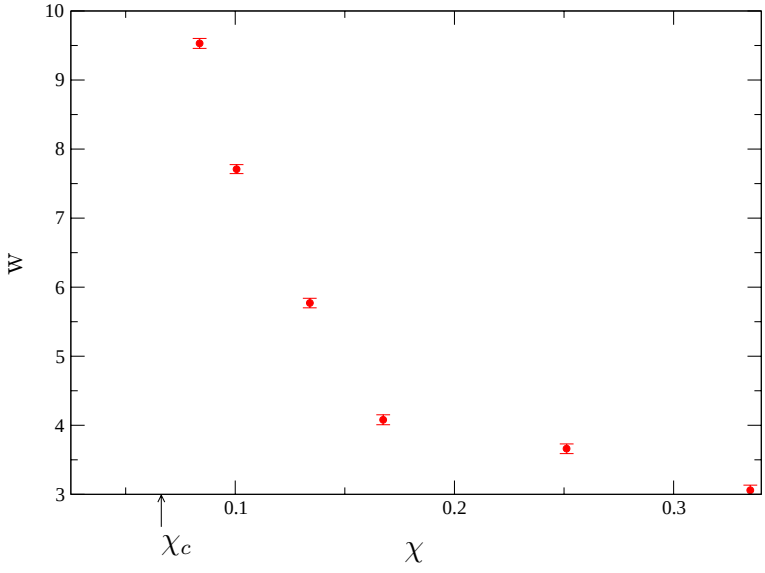

Figure 4.24: Total interfacial width as a function of the interaction parameter, χ for flexible and semiflexible with persistence length ($\frac{l_p}{a} = 2.5$). Arrow marks the critical value of χ, estimated using the data of interfacial tension.

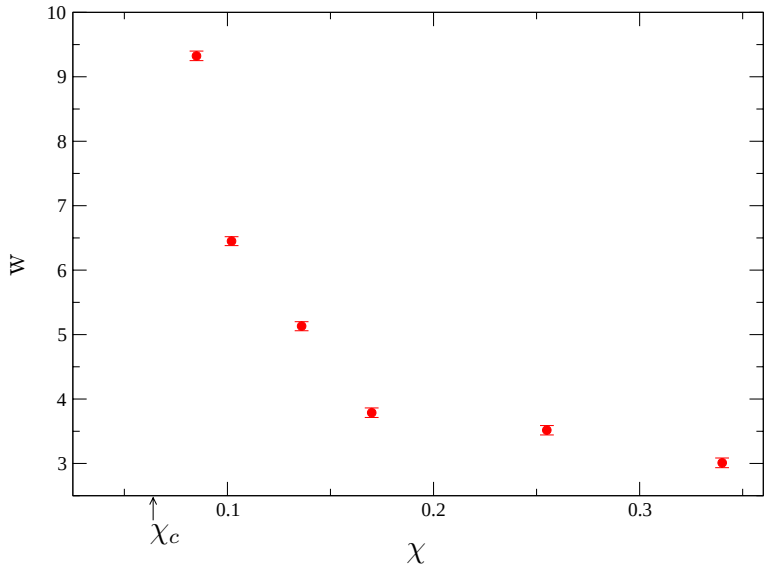

Figure 4.25: Total interfacial width as a function of the interaction parameter, χ for flexible and semiflexible with persistence length ($\frac{l_p}{a} = 4.2$). Arrow marks the critical value of χ, estimated using the data of interfacial tension.

with the decrease in the interfacial tension. The interfacial width will be infinite at the critical value of χ.

4.4.3 Estimation of Critical Value of χ

As described above we have estimated the critical value of χ as a function of stiffness of semiflexible component in our systems of study. We have carried out the study of flexible-flexible polymer blend and flexible-semiflexible (with varying persistence lenth up to 4.2) polymer blends. First, we studied the dependence of interfacial tension on Flory-Huggins parameter χ by reducing value of χ from strong segregation limit. The data are compared with mean-field expressions in equations 4.15 keeping the same mean-field exponents. Further comparison of our estimated value of critical χ with that of Werner *et al.* [81] for the flexible-flexible polymer blend shows that our result for this system ($\chi_C = 0.0795$) are not much different from their result ($\chi_C = 0.08$, estimated from their graph).

Figure 4.27 shows the ratio of critical temperature for a system with flexible-semiflexible chains to that of flexible-flexible system. It can be seen from the figure that the critical temperature increases with the increase in stiffness of semiflexible components.

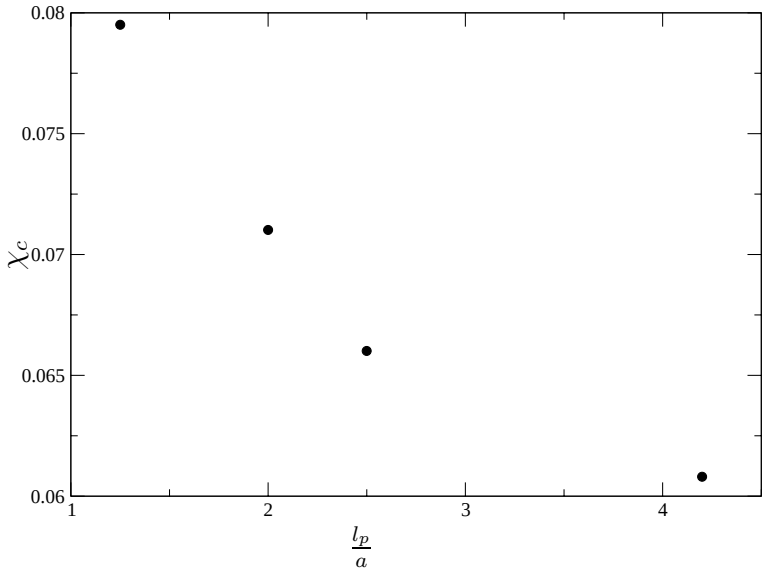

Figure 4.26: critical value of F-H parameter as a function of stiffness of the semiflexible component. Here the persistence length are in units of bond length.

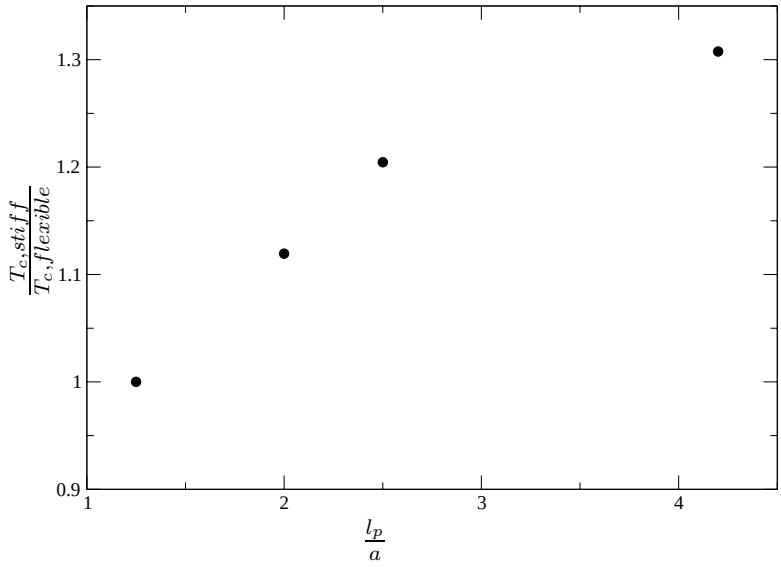

Figure 4.27: Ratio of critical temperature of semiflexible-flexible system to flexible-flexible system as a function of stiffness of the semiflexible component. Here the persistence length are in units of bond length.

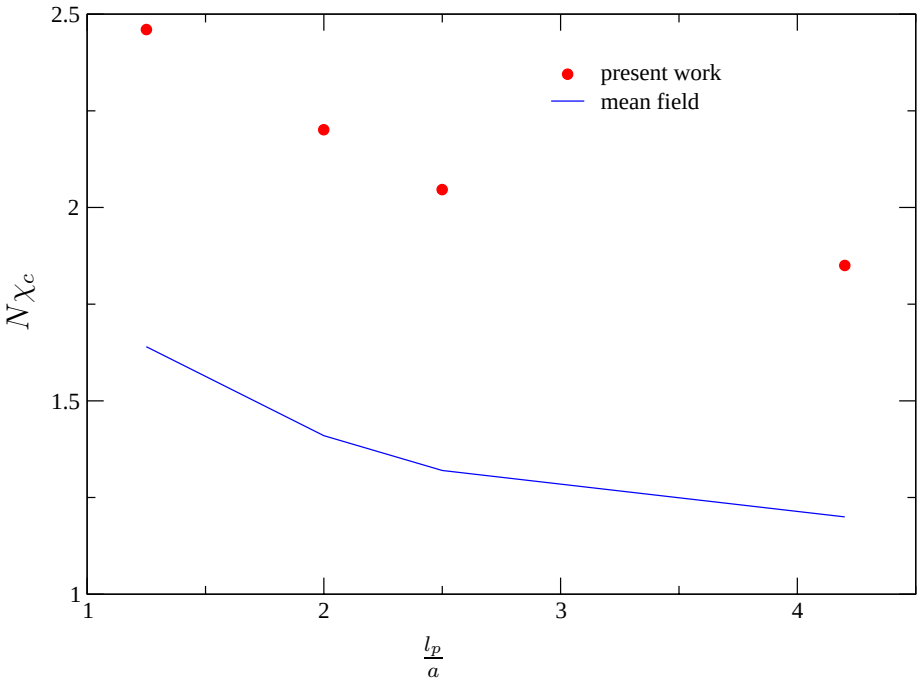

Figure 4.28: $N\chi_c$ as a function of stiffnes of the semiflexible components.

The data have been compared to mean filed. From mean filed theory, one gets [1],

$$N\chi_c = \frac{1}{2}\left(\frac{1}{(C_{1NA})^{\frac{1}{4}}} + \frac{1}{(C_{1NB})^{\frac{1}{4}}}\right)^2 \tag{4.17}$$

where C_{1Ni} $(i = A, B)$ is the characteristic ratio as defined in chapter 3 of ith component and N is the number of monomers in a chain. The value of $N\chi_c$ as a function of stiffness of the semiflexible component, in the blend of flexible-semiflexible polymers, has been calculated using above formula and from simulation data. Figure 4.28 shows both the data. Both data show that the value of $N\chi_c$ decreases with increase in stiffnes of the semiflexible polymers. The mean filed theory gives lower values of $N\chi_c$ in comparison to simulation which is not unexpected as the mean field theory neglects the fluctuations. The nature of both data is the same.